

FBG inscription by a biprism interferometer: analysis and experiment

R. Mahakud¹  · J. Kumar¹ · O. Prakash¹ · S. K. Dixit¹ · S. V. Nakhe¹

Received: 10 March 2015 / Accepted: 20 September 2015 / Published online: 5 October 2015
© Springer-Verlag Berlin Heidelberg 2015

Abstract In this paper, the effect of spatial variation of fringe visibility on the length, reflectivity and wavelength tuning of fiber Bragg gratings (FBGs), written by a biprism interferometer, is analyzed. The variation of fringe visibility and usable fringe area are the cumulative effect of spectral and spatial frequency spectrum of the laser source, beam profile and fringe stability. It is analytically shown that with the increase in the distance of FBG writing plane from the biprism, the saturation of UV fringes-induced refractive index modulation decreases, whereas the reflectivity of FBGs inscribed will pass through a maximum. Fiber Bragg gratings are written by a UV beam (255 nm, 5.6 kHz, 30 ns) at different distances from a 24° refraction angle biprism. The trends on experimental results matched the analysis. The maximum reflectivities observed are of 93.6 % (12 dB) for FBGs in Ge-B co-doped fiber and 99.8 % (29 dB) for FBGs in hydrogen-loaded SMF-28 fiber, attributed to the consideration of spatial variation of fringe visibility in the biprism fringe depth on the optimization of FBG reflectivity. These are incidentally the highest values, so far reported, for FBGs written by a biprism interferometer.

1 Introduction

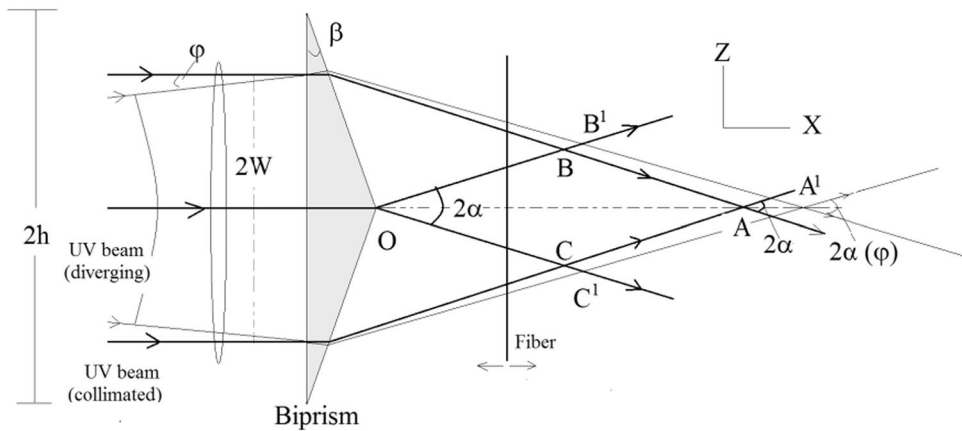
Fiber Bragg gratings (FBGs) are important components in fiber optic communication and sensor systems [1–3]. Fiber

Bragg grating is made by inducing refractive index (RI) modulation, by spatially patterned UV radiation, in the core of a photosensitive optical fiber [4–8]. Phase mask, interferometric and point-by-point methods are used for FBG fabrication. Phase mask technique is most efficient, but wavelength specific. Distributed sensing requires multiplexing of many FBGs, each of different Bragg wavelengths, in the fiber network. Both phase mask—Talbot interferometer and point-by-point technique are suitable for writing FBGs at different Bragg wavelengths [9–12]. The long arm of Talbot or mirror-based interferometers necessitates a stable UV beam for multi-pulse FBG inscription. The stability of fringe system in a mirror-based interferometer, involving large number of optical and mechanical components, is prone to environmental disturbances. Submicron focal spot and positional accuracy of translation stages are required for fabrication of submicron period FBG by the point-by-point method. FBG fabrication by focused femto-second laser by point-by-point method relies on refractive index changes by multi-photon absorption [12]. Such FBGs reveal large birefringence and high degree of polarization. The prisms interferometers, simple and cost effective, are used as a method of wavefront division to holographically write first-order Bragg gratings [13–16]. A biprism interferometer offers many advantages such as high damage threshold in the absence of surface coatings, inherent fringe stability due to a single optical element, ease of fabrication and handling and suitable for Bragg wavelength tuning. FBGs at different Bragg wavelengths can be inscribed by the same biprism using a geometrically diverging UV beam incident on the biprism [17]. The tuning is accomplished by translation of the fiber in the biprism fringe depth, which avoids the necessity to rotate the biprism or changing the angle of incidence of the UV beam. The tuning can also be accomplished by changing the geometrical divergence

✉ R. Mahakud
rkmahakud@rrcat.gov.in

¹ Metal Vapour and Dye Laser Applications Laboratory,
Laser Systems Engineering Section, R&D C3 Block, Raja
Ramanna Centre for Advanced Technology (RRCAT),
Indore 452013, India

Fig. 1 Schematic of FBG writing by a biprism interferometer



envelope of the UV beam. The fiber is then placed in a particular position, particularly in the fringe plane of optimum FBG reflectivity. However, the reported reflectivities of biprism-written FBGs are low [13–15]. The FBG reflectivity observed in biprism-based writings is: 44 % with the frequency-doubled (244 nm) CW Ar⁺ laser [13], 62 % with single-pulse writing by excimer laser (248 nm) [14] and 55 % with frequency-doubled (255 nm) copper vapor laser [15]. In the above studies, fiber-to-biprism distance was fixed; particularly, fiber was placed at the middle of the fringe depth to obtain maximum FBG length. However, the effect of spatial variation of fringe visibility in the biprism fringe depth on saturation of RI modulation, limitation of FBG length and reflectivity needs to be addressed.

In this paper, the effect of spectral and spatial frequency spectrum of the laser source on the spatial variation of fringe visibility and the usable fringe area in the beam overlap region of a biprism is analyzed in view of writing fiber Bragg gratings. The effect of spatial variation of fringe visibility on limitation of length, reflectivity and wavelength tuning of gratings written is discussed. The FBGs were written at different distances from the biprism by a low-pulse-energy and high-repetition-rate UV (255 nm, 5.6 kHz, 30 ns, 55 μJ) beam. Experimental results observed agreed with the analysis.

2 FBG writing by a biprism interferometer

Figure 1 shows the cross-sectional view of UV beams (thick ray for collimated and thin ray for diverging beam) incident on the biprism of width $2h$, refractive angle β and material refractive index n_p . The biprism is having an axial symmetrical structure with a rectangle aperture. The apex of the biprism (O) is taken as origin, and x -axis as optical axis. The z -axis is defined along the wedge angle direction vertical to the x -axis on the plane. The laser source photon energy lies in the absorption band of the GeO defects in the

fiber. The biprism divides the incident UV beam of width $2W$ (in xz -plane) into two halves. For the collimated beam, the fringes are formed in the diamond-shaped overlap region OBAC [co-ordinates O (0, 0), A ($2x_0$, 0), B (x_0 , z_0) and C (x_0 , $-z_0$)]. Different angles and optical path lengths in the interferometer geometry are calculated by ray optics.

As shown in Fig. 1, the beam overlap length along optical axis (OA) for the collimated beam is $2x_0$ and that transverse to optical axis (BC) is $2z_0 (= 2x_0 \tan \alpha)$ where x_0 (distance of maximum overlap plane from O) and α (angle of intersection of the refracted ray with x -axis) are given as,

$$x_0 = 0.5W(\cot \alpha - \tan \beta); \quad \alpha = \sin^{-1}(n_p \sin \beta) - \beta \quad (1)$$

For FBG inscription, the fiber is placed in a fringe plane (x) parallel to z -axis. The UV fringes-exposed fiber length, $L(x)$, is given as,

$$L(x) = 2x \tan \alpha \text{ (for } x \leq x_0) \quad \text{and} \quad (2x_0 - x) \tan \alpha \text{ (for } x_0 < x < 2x_0) \quad (2a)$$

The fringe width (Λ) is given as,

$$\Lambda = \lambda_{uv}/2 \sin \alpha \quad (2b)$$

The Bragg wavelength (λ_b) in the first order of a inscribed FBG is given as, $\lambda_b = 2n_{\text{eff}} \Lambda$, where n_{eff} is effective refractive index of the fiber. Separate biprisms of different refraction angles are required to write FBGs at different wavelengths. However, FBGs at different Bragg wavelengths with considerable tunability can be inscribed when a geometrically diverging UV beam of small angular envelope incident on the biprism. The fringes are formed in the overlap region OB¹A¹C¹. In this case, the loci of fringes are hyperbolic, like those in the Young's double slit. The fringe width will increase with the increase in the distance (x) of the fringe plane from the biprism [17]. Figure 2 shows the variation of Bragg wavelength with the increase in the distance of separation between fringe plane and biprism for inputs $h = 10$ mm, $W = 6$ mm, $n_p = 1.5$, $n_{\text{eff}} = 1.456$, $\beta = 24^\circ$ for $2\phi = 0, 10$ and 2° . With the increase in the

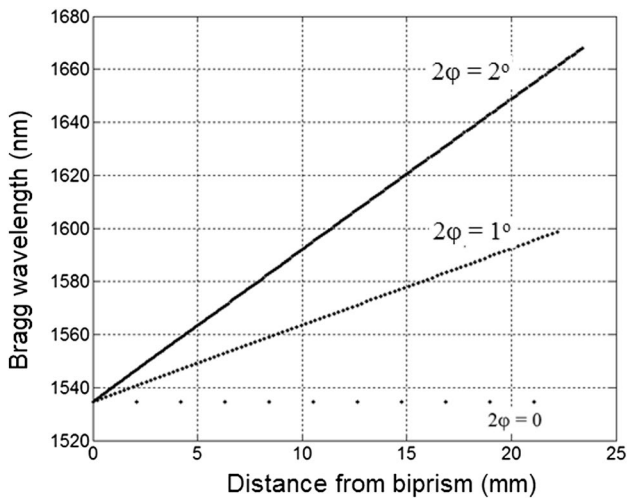


Fig. 2 Change in Bragg wavelength with the increase in the distance (x) from the biprism

biprism-to-fiber distance (x) from O to A^1 , the change in Bragg wavelength is of about 67 nm ($d\lambda_b/dx \sim 2.9$ nm/mm for $2\phi = 1^\circ$) and 134 nm ($d\lambda_b/dx \sim 5.8$ nm/mm for $2\phi = 2^\circ$).

For fully coherent UV beam, the FBGs could be written at any position in the fringe depth. However, depending on the coherence properties of the light source, the usable interference region for FBG inscription may be reduced as compared to the diamond-shaped beam overlap region. The restrictions are especially due to spatial variation of fringe visibility.

2.1 Spatial variation of fringe visibility

The intensity distribution in the interference region can be described as,

$$I(x, z) = I_1(x, z) + I_2(x, z) + 2\sqrt{I_1(x, z)I_2(x, z)}|\gamma_{12}(x, z)| \cos[k_{uv}\Delta l] \tag{3}$$

where Δl is optical path difference, $k_{uv} (= 2\pi/\lambda_{uv})$ is propagation constant, $I_1(x, z)$ and $I_2(x, z)$ are intensity distributions, $|\gamma_{12}(x, z)|$ is the normalized mutual coherence of light field. The fringe visibility (V) is given as,

$$V(x, z) = g(x, z)|\gamma_{12}(x, z)| \tag{4}$$

where $g(x, z) = 2 \{I_1(x, z) I_2(x, z)\}^{1/2} / \{I_1(x, z) + I_2(x, z)\}$, termed as fringe modulating parameter further in the text. For a perfectly coherent beam, $|\gamma_{12}(x, z)| = 1$ and $0 \leq |\gamma_{12}(x, z)| \leq 1$ for a partially coherent source. The normalized mutual coherence in a typical fringe plane depends on statistical properties of the source and geometry of

the interferometer setup. The mutual degree of coherence combines both spatial and temporal characteristics in one single term. Spatial coherence is the correlation of the electric fields at two different positions (r_1 and r_2) on the same wave front. Temporal coherence is the correlation between the fields at two different times (t_1 and $t_2 (= t_1 + \tau)$) in the same wave train. The time average fringe visibility is cumulative effect of spectral and spatial frequency spectrum of the laser source, intensity distribution across the beam and fringe stability.

2.1.1 Effect of finite spatial coherence

For a source with continuous spectrum, the normalized mutual coherence is the Fourier transform of the spectral and spatial frequency spectrum of the laser source [18]. The Fourier transform of a Gaussian distribution of spatial frequency spectrum is a Gaussian and that for a flat top spectrum is a Sinc correlation function, and it decreases with the increase in the separation distance between two interfering points emanating from the same wavefront [18–20]. The distance of separation (r_s) between two points on the incident wavefront (in case of collimated beam) from which emanating waves interfere at $P(x, z)$ is given as,

$$r_s = \frac{2x \tan \alpha}{1 - \tan \alpha \cdot \tan \beta} \tag{5}$$

In case of a geometrically diverging UV beam, the distance x is higher for same distance of separation between two points on the wavefront incident on the biprism. Thus the normalized mutual coherence will decrease with the increase in distance of the fringe plane (x) from the biprism. Assume that the incident beam is a composite of a finite angular spectrum of plane waves originating from the extended source at angles ($\delta\theta$) varying between $-\Delta\phi/2$ and $+\Delta\phi/2$ where $\Delta\phi$ is diffraction divergence of the UV beam. By incorporating the angular dependence of k -vector, the additional phase difference [$\delta(k\Delta l)$] introduced at a point of interference between two plane waves, originating at angle $\delta\theta$ from the extended source, is $\sim k_{uv}(r_s\delta\theta)$. Integration of fringe intensity, over all $\delta\theta$ in between $-\Delta\phi/2$ and $+\Delta\phi/2$, and the normalized mutual degree of coherence for a flat top spatial frequency distribution can be described as,

$$|\gamma_{12}(x, \Delta\phi)| \approx \left| \text{Sinc} \left[\frac{k_{uv}x \tan \alpha \Delta\phi}{1 - \tan \alpha \cdot \tan \beta} \right] \right| \tag{6}$$

The fringe visibility will decrease with the increase in the beam divergence, refraction angle of the biprism and distance of the fringe plane from the biprism. The change of $|\gamma_{12}(x, \Delta\phi)|$ and $L(x)$ with the increase in x for inputs $\beta = 24^\circ$, $W = 6$ mm, $\Delta\phi = 25$ and $100 \mu\text{rad}$ is shown in Fig. 3 as an illustration.

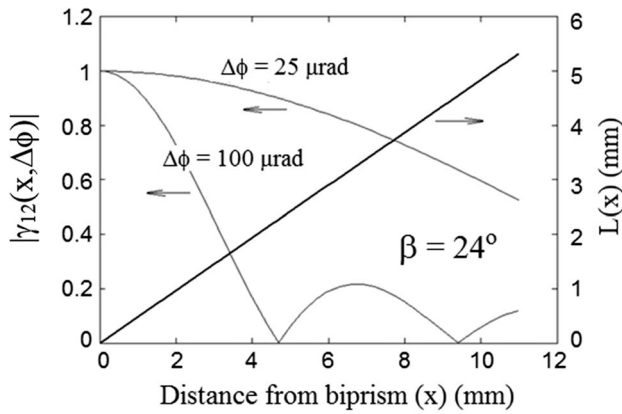


Fig. 3 Variation of simulated normalized mutual degree of coherence $|\gamma_{12}(x, \Delta\phi)|$ and exposure length $[L(x)]$ with the increase in distance (x) from the biprism

2.1.2 Effect of finite temporal coherence

A sinusoidal fringe pattern is formed for a single temporal frequency of the UV beam. However, for a source with finite temporal coherence, the integration of sinusoidal fringe intensity (Eq. 3) over whole spectral width $(\Delta\nu)$ will lead to change in fringe intensity, along z -axis (Fig. 1). The normalized mutual temporal coherence, for a source with flat temporal frequency spectrum, can be expressed as, $|\gamma_{12}(\Delta\nu, \tau)| \sim |\text{Sinc}(\pi\Delta\nu\tau)|$, where $\tau (= \Delta l/c$ where c is velocity of light) is time delay. In the present setup (Fig. 1), $\tau = \xi z/c$ where $\xi = 2\tan\beta$ ($\sec\alpha - n_p$)/($1 - \tan\alpha \cdot \tan\beta$). Thus, $|\gamma_{12}(\Delta\nu, z)|$ can be expressed as,

$$|\gamma_{12}(\Delta\nu, z)| = \left| \text{Sinc} \frac{\pi \Delta\nu \xi z}{c} \right| \tag{7}$$

The fringe visibility will decrease with the increase in the distance $(|z|)$ from the optical axis. Figure 4 shows the variation of $|\gamma_{12}(\Delta\nu, z)|$ with z for spectral bandwidths of 10 GHz (2.1 pm), 240 GHz (50.4 pm) and 500 GHz (105 pm) with inputs $W = 6$ mm, $n_p = 1.5$ and $\beta = 24^\circ$. The decrease in $|\gamma_{12}(\Delta\nu, z)|$ with z is steeper for higher spectral bandwidth of the laser source.

2.1.3 Effect of beam profile

For uniform beam profile, the fringe modulating parameter $[g(x, z)]$ is unity. However, for a non-uniform beam profile such as cylindrically focussed top hat or a Gaussian UV beam, the field amplitude at $P(x, z)$ is not same for both the refracted beams as they originate from different points on the wavefront, separated by the distance r_s . The spatial variation of fringe modulating parameter will be different for

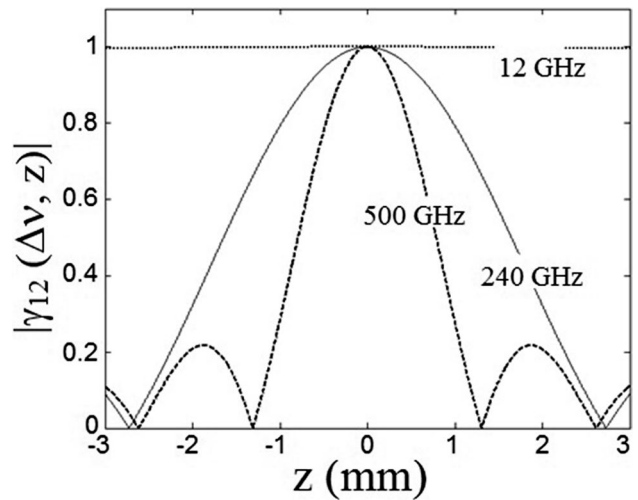


Fig. 4 Variation of simulated normalized mutual degree of coherence $|\gamma_{12}(\Delta\nu, z)|$ with the increase in distance (z) from optical axis $(z = 0)$ for different spectral widths

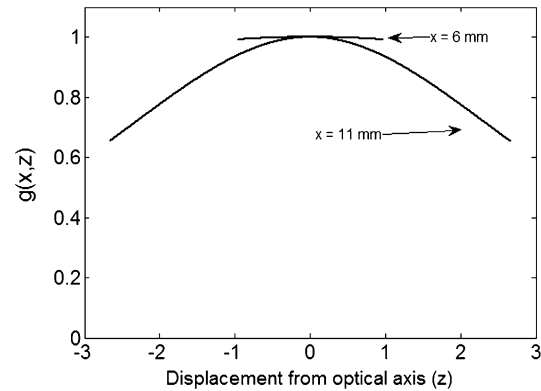


Fig. 5 Variation of simulated fringe modulating parameter $[g(x, z)]$ with the increase in distance (z) from optical axis at $x = 6$ mm and $x = 11$ mm

different beam profiles and different FBG writing planes in the fringe depth. As an illustration, for a Gaussian beam, $g(x, z)$ can be expressed as,

$$g(x, z) = \frac{2e^{-(b_1^2 + b_2^2)/W^2}}{e^{-2b_1^2/W^2} + e^{-2b_2^2/W^2}} \tag{8}$$

where $b_1 = (x \tan\alpha + z)/(1 - \tan\alpha \cdot \tan\beta)$ and $b_2 = (x \tan\alpha - z)/(1 - \tan\alpha \cdot \tan\beta)$. Figure 5 shows the variation $g(x, z)$ along z in the typical fringe planes at $x = 6$ mm and $x = 11$ mm for inputs $\beta = 24^\circ$ and $W = 6$ mm. The fringe modulating parameter decreased from unity at $z = 0$ to about 0.66 at $z = \pm 2.6$ mm. It is clear that the variation of $g(x, z)$ is different in different fringe planes.

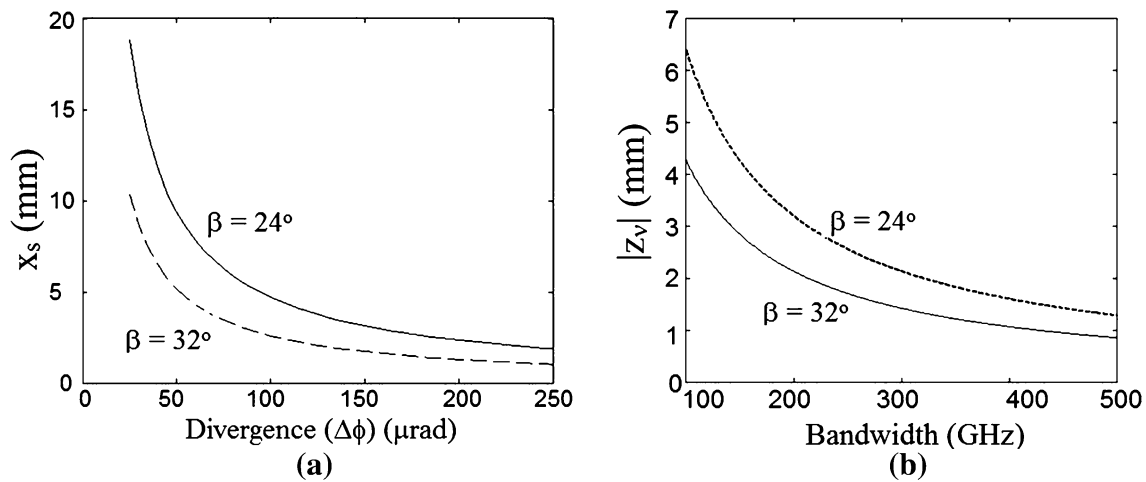


Fig. 6 Variation of the **a** distance (x_s) of the zero visibility with diffraction divergence ($\Delta\phi$) along optical axis and **b** distance ($|z_v|$) of the zero visibility with spectral bandwidth ($\Delta\nu$) normal to the optical axis

2.1.4 Effect of fringe stability

The stability of fringes depends on acousto-optic vibration, ambient temperature fluctuation and laser beam pointing instability. In a biprism interferometer, the fringe drift due to beam pointing instability increases with the increase in the distance of the fringe plane from the biprism [21]. For single-pulse writing of FBG, the fringe stability is immaterial. But FBG writing requires millions of pulses for a low pulse energy laser beam or tens of seconds for a CW beam. The spatial shifting of fringes with respect to the fiber will dilute the refractive index modulation contrast of the FBG requiring 10 s of seconds for inscription.

2.2 Effect spatial variation of fringe visibility on FBG parameters

2.2.1 FBG length

The variation of fringe visibility along x and z directions will limit the usable fringe area for FBG inscription. The UV beam of higher divergence ($\Delta\phi$) restricts the FBG length via the maximum permissible distance of the fiber from the biprism. A uniform UV beam with a flat top distribution of spatial and spectral frequency spectrum is considered for calculation of FBG parameters. The distance of first zero fringe visibility (x_s) from the biprism apex (O), from Eq. (6), is given as,

$$x_s = \lambda_{uv}(1 - \tan \alpha \cdot \tan \beta)/2\Delta\phi \tan \alpha \tag{9}$$

For $x_s > 2x_0$, the diffraction divergence is not a limitation on FBG length. However, for $x_s < 2x_0$, the distance x_s may be assumed as the maximum permissible distance, between biprism and fiber, for FBG inscription. The UV beam far-field divergence may be reduced by different techniques

such as spatial filtering, expanding the beam diameter or by changing the optical resonator of the source laser. The biprisms of different refraction angles may be used to write FBGs at different Bragg wavelengths. Figure 6a shows the variation of x_s versus $\Delta\phi$ for $\beta = 24^\circ$ and $\beta = 32^\circ$. The maximum permissible distance from biprism to fiber decreases with the increase in beam divergence ($\Delta\phi$) and biprism refraction angle (β).

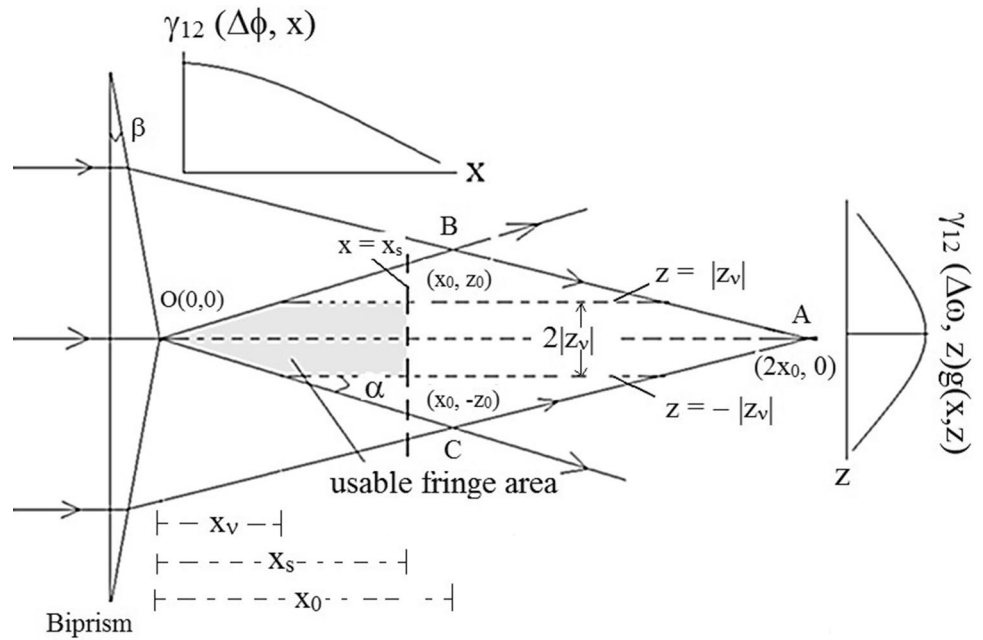
The large spectral width of the writing UV beam may limit the FBG length. The distance ($|z_v|$) of the position of zero fringe visibility, along z , from the optical axis is given as,

$$|z_v| = c/\xi \Delta\nu \tag{10}$$

Figure 6b shows the change of $|z_v|$ with change in UV beam spectrum bandwidth ($\Delta\nu$) for $\beta = 24^\circ$ and $\beta = 32^\circ$. The spectral width ($\Delta\nu$) will not limit the usable fringe area for $|z_v| > z_0$ [for which $\Delta\nu < (c/\xi z_0) = (c/\xi x_0 \tan \alpha)$]. Typically, $z_0 (=x_0 \tan \alpha)$ is 2.67 mm for $\beta = 24^\circ$ and 2.3 mm for $\beta = 32^\circ$ for inputs $W = 6$ mm and $n_p = 1.5$. In such a case, the spectral bandwidth will not restrict the FBG length for $\Delta\nu < 240$ GHz (for $\beta = 24^\circ$) and $\Delta\nu < 206$ GHz (for $\beta = 32^\circ$). However, for $\Delta\nu > (c/\xi z_0)$, the maximum possible length of FBG will depend on spectral bandwidth ($\Delta\nu$) of the source. Inscription of FBGs beyond maximum overlap ($x > x_0$) is not preferable as both fringe contrast and FBG length decrease. Incorporating both the spatial and temporal effect, the maximum length (L_{max}) of a FBG that can be inscribed by placing the fiber in the biprism fringe depth may be expressed as,

$$L_{max} = \begin{cases} 2c/\xi \Delta\nu & (x_v < x_s < x_0) \\ 2x_s \tan \alpha & (x_s < x_v < x_0) \\ 2x_0 \tan \alpha & (x_v \geq x_s > x_0) \end{cases} \tag{11}$$

Fig. 7 Pictorial representation of usable fringe area in the overlap region



where $x_v = (c/\xi \Delta v \tan \alpha)$.

Figure 7 is a pictorial representation of the region of usable area of interference region (shaded) for FBG inscription for $x_v < x_s < x_0$. The horizontal dotted lines ($z = \pm |z_v|$) parallel to optical axis represent the positions of zero fringe visibility in the fringe planes, transverse to optical axis. The vertical dotted line ($x = x_s$) represents zero fringe visibility plane perpendicular to optical axis. For UV sources of different beam profiles and temporal and spatial frequency spectrum, the spatial variation of fringe visibility may be different. Typically, for a Gaussian distribution, the fringe visibility will decrease exponentially with the increase in x and z . In such cases, x_s and $|z_v|$ may be assumed as the distance where the fringe visibility reduces to e^{-2} of that at $x = 0$ and at $z = 0$, respectively. The variation of fringe modulating parameter and fringe instability will further reduce the useable fringe area, thus affecting both FBG length and reflectivity.

2.2.2 Refractive index (RI) modulation

The physical mechanisms behind UV-induced refractive index changes are not completely understood and can greatly vary depending upon exposure conditions and glass composition. A proposed model of UV fringes-induced refractive index distribution is of the form [16],

$$\delta n(z, N) = \Delta n_0 \left[1 - e^{-kN[1 + \cos(2\pi z/\Lambda)]} \right] \tag{12}$$

where Δn_0 is saturable index change, N is the number of incident UV pulses and k is a fitting parameter [16]. The fitting parameters are likely to involve absorption cross

section of defects at the UV wavelength and intensity of the incident UV radiation. As per Eq. (12), the induced refractive index at position of fringe minimum is zero. This is true for UV fringes of unity visibility only. To incorporate spatial variation of fringe visibility, as in case of FBG writing by a biprism interferometer, the modified form of Eq. (12) may be expressed as [22]

$$\Delta n(x, z) = \Delta n_0 \left[1 - e^{-\chi F_0 [1 + V(x, z) \cos(\frac{2\pi}{\Lambda} z)]} \right] \tag{13}$$

where $\Delta n(x, z)$ is the distribution of RI change, $V(x, z)$ is fringe visibility, $F_0 (=NI_0\tau_p)$, N is the number of incident UV pulses, $I_0(x, z)$ is fringes mean intensity and τ_p is pulse duration) is mean fluence and χ is a constant. Equation (13) is based on single-quantum excitation to the UV absorption band (usually, 5 eV) of germanium-oxygen-deficient centers in the fiber core, and the RI change is proportional to depletion of germanium-oxygen-deficient centers (GODCs) depleted on UV absorption. The constant parameter $\chi (= \sigma/h\nu_{uv})$ depends on absorption cross section (σ) of GODCs at incident UV wavelength. The UV fringes-induced RI distribution along the fiber length is a function of fringe visibility and fluence. Δn_0 is the maximum RI change possible in the fiber core subject to UV illumination. The UV fringes-induced RI profile deviates from sinusoidal due to nonlinear growth. The Fourier expansion of RI change is given as,

$$\begin{aligned} \Delta n(x, z) = & \langle \Delta n(x, z) \rangle + \Delta n_{ac}(x, z) \cos\left(\frac{2\pi}{\Lambda} z\right) \\ & + \Delta n^{(2)}(x, z) \cos\left(\frac{4\pi}{\Lambda} z\right) + \Delta n^{(3)}(x, z) \cos\left(\frac{6\pi}{\Lambda} z\right) + \dots \end{aligned} \tag{14}$$

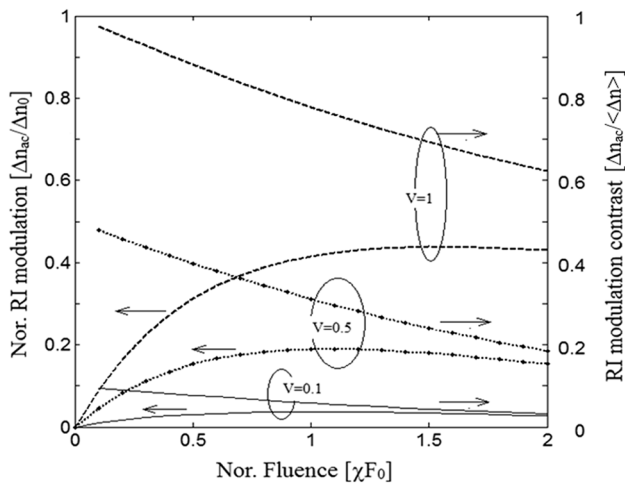


Fig. 8 Variation of simulated normalized RI modulation and RI modulation contrast with the increase in the normalized fluence for different fringe visibilities ($V = 0.1, 0.5$ and 1)

where $\langle \Delta n(x, z) \rangle$ is 0th component and $\Delta n_{ac}(x, z)$, $\Delta n^{(2)}(x, z)$ and $\Delta n^{(3)}(x, z)$ are amplitudes of first, second and third harmonics of Fourier expansion of $\Delta n(x, z)$, respectively. The coefficients of harmonic terms in Eq. (14) depend on x and z due to variation of fringe visibility and fringe mean intensity. The FBG reflection in first order is due to first harmonic of $\Delta n(x, z)$ in which $\Delta n_{ac}(x, z)$ is termed as RI modulation. $\langle \Delta n(x, z) \rangle$ is the period-averaged RI change. The average RI change and the RI modulation are given as,

$$\begin{aligned} \langle \Delta n(x, z) \rangle &= \frac{1}{\Lambda} \int_0^\Lambda \Delta n(x, z) dz; \\ \Delta n_{ac}(x, z) &= \frac{2}{\Lambda} \int_0^\Lambda \Delta n(x, z) \cos\left(\frac{2\pi}{\Lambda}z\right) dz \end{aligned} \tag{15}$$

The solutions of Eq. (15), obtained numerically, describe the growth of normalized RI modulation and average refractive index change with fluence. Figure 8 shows simulated variation normalized RI modulation $[\Delta n_{ac}/\Delta n_0]$ and RI modulation contrast $[v = \Delta n_{ac}/\langle \Delta n \rangle]$ with the increase in normalized fluence (χF_0) for typical visibility of $V(x, z) = 0.1, 0.5$ and 1 . The visibility of fringes decreases with the increase in distance x from the biprism and distance z from optical axis.

The point (x, z) refers to a differential section on the fiber centered at a point $P(x, z)$. In this differential section, the visibility is treated as constant with its value varying in between 0 and 1 depending on x and z . The RI modulation contrast is defined as the ratio of RI modulation to the period-averaged RI change. The growth and saturation of RI modulation with fluence is higher for UV fringes of

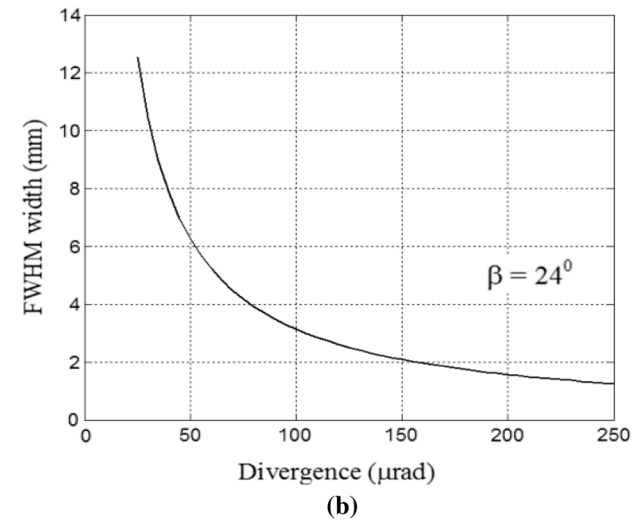
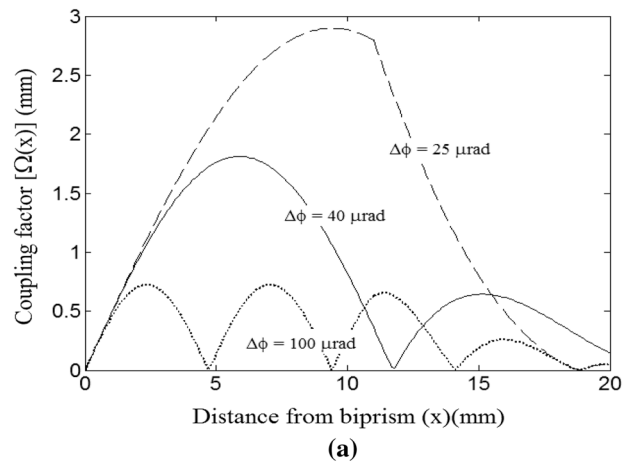


Fig. 9 Variation of simulated **a** coupling factor $[\Omega(x)]$ with the increase in the distance (x) of the fringe plane from the biprism **b** FWHM width (Δx) of $\Omega(x)$ with the increase in diffraction divergence ($\Delta\phi$) of the UV beam for $\beta = 24^\circ$

higher contrast. The RI modulation contrast decreased with the increase in fluence due to both nonlinear growth and decrease in fringe visibility.

2.2.3 FBG reflectivity

In the process of FBG inscription, the spatial variation of fringe visibility leads to spatial variation of refractive index modulation. Thus change in FBG length and RI modulation with the increase in distance from the biprism needs to be taken into account for optimization of FBG writing by a biprism interferometer. The net fringe visibility may be expressed as,

$$V(x, z) = g(x, z) |\gamma_{12}(\Delta\phi, x)| |\gamma_{12}(\Delta\nu, z)| \tag{16}$$

A uniform FBG is formed for a sufficiently narrow line width ($|\gamma_{12}(\Delta\nu, z)| \sim 1$) and a uniform UV beam [$g(x,$

$z) \sim 1]$. The FBG reflectivity (R) of a uniform FBG at resonance is given as [2],

$$R = \tanh^2(\kappa L) \tag{17}$$

where L is grating length, $\kappa (= \pi\eta\nu <\Delta n>/\lambda_b)$ is coupling coefficient, η is mode overlap integral, and ν is modulation contrast. The techniques of transfer matrix or multilayer analysis are used to simulate FBG reflectivity in case of variation of RI modulation along FBG length [2]. However, even for UV beams of large spectral bandwidth, the maximization of FBG reflectivity requires maximizing the quantity, $\Omega(x) = [V(x, 0)L(x)]$. The term $[\Omega(x)]$, designated as the coupling factor, is the upper limit of $[\nu(x,0)L(x)]$. The coupling factor $[\Omega(x)]$ for a flat spatial spectrum can be expressed as,

$$\Omega(x) \approx \begin{cases} \Omega_0 \sin\left(\frac{\kappa_{uv}x\Delta\phi \tan\alpha}{(1-\tan\alpha \cdot \tan\beta)}\right) & (x < x_0) \\ \Omega_0\left(\frac{2x_0}{x} - 1\right) \sin\left(\frac{\kappa_{uv}x\Delta\phi \tan\alpha}{(1-\tan\alpha \cdot \tan\beta)}\right) & (x \geq x_0) \end{cases} \tag{18}$$

where $\Omega_0 = [\lambda_{uv} (1 - \tan\alpha \cdot \tan\beta)]/\pi\Delta\phi$. Figure 9a shows $\Omega(x)$ versus x for different values of $\Delta\phi$ (mentioned in the figure). In case of a Gaussian distribution, there will be one maximum in $\Omega(x)$ versus x . The distance (x_m) of the fringe plane at which $\Omega(x)$ is maximum $[=\Omega_0]$ is given as,

$$x_m = \lambda_{uv}(1 - \tan\alpha \cdot \tan\beta)/4\Delta\phi \tan\alpha \tag{19}$$

Ω_0 is the value of $\Omega(x)$ in the fringe plane at a distance, $x = x_m$, from the biprism. Thus the unit of Ω_0 is same as that of $\Omega(x)$. The units of both Ω_0 and x_m are that of length, similar to laser beam spatial coherence width ($\sim\lambda/\Delta\phi$ where $\Delta\phi$ is far-field beam divergence). Both Ω_0 and x_m decrease with the increase in beam divergence ($\Delta\phi$). The distance x_m is about half the distance of zero visibility (x_s) fringe plane from the biprism.

With the increase in beam divergence increasing from 25 to 100 μrad , Ω_0 will decrease from 2.9 to 0.72 mm and x_m will decrease from 9.7 to 2.4 mm for inputs, $W = 6$ mm and $\beta = 24^\circ$. Thus it is clear that the fringe plane at maximum beam overlap position ($x_0 \approx 11$ mm) in the overlap region is not necessarily the FBG writing plane of maximum reflectivity. The FWHM width (Δx) of $\Omega(x)$ is $2x_m/3$ for $x_m < x_0/2$ and between $x_m/3$ and $2x_m/3$ for $x_m \geq x_0/2$. Figure 9b shows variation of FWHM width (Δx) of $\Omega(x)$ versus $\Delta\phi$ for a collimated beam ($\varphi = 0$) for $\beta = 24^\circ$. Typically the FWHM width decreased from about 12 mm for $\Delta\phi = 25 \mu\text{rad}$ to 2 mm for $\Delta\phi = 150 \mu\text{rad}$. The FWHM width of $\Omega(x)$ is important for FBG writing at different Bragg wavelengths by a diverging UV beam. The role of geometrical and diffraction (far-field) divergence is different ($2\varphi \neq \Delta\phi$). The diffraction divergence ($\Delta\phi$) is an inherent property of the laser source, related to its spatial coherence. This determines the visibility of fringes in a typical interferometer. The geometrical divergence is linked

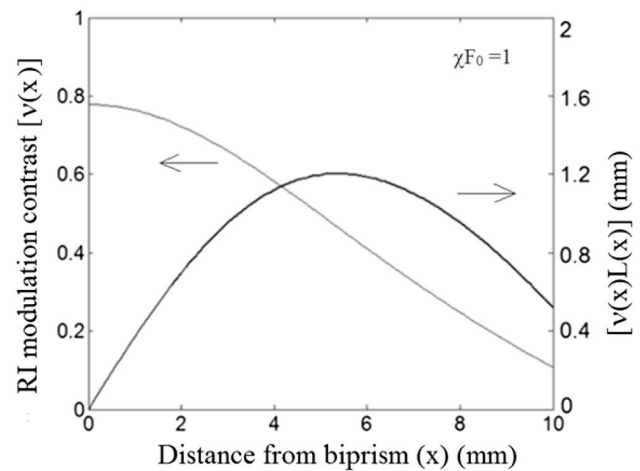


Fig. 10 Variation of simulated RI modulation contrast $[v(x)]$ and $[v(x)L(x)]$ with the increase in the distance (x) of the FBG writing plane from the biprism

with the curvature of the wavefront which can be always compensated by suitable optics leading to collimated (plane wavefront) beam. The locus of the fringes depends on geometrical divergence (2φ). In a biprism interferometer, the fringes are parallel for $2\varphi = 0$ (collimated beam) and hyperbolic for $2\varphi \neq 0$ (diverging beam). The large geometrical divergence will affect the fringe visibility via the distance of separation between two points (r_s) on the wavefront incident on the biprism from which the emanating waves interfere at a point $P(x, z)$ in the fringe plane. It is apparent from Fig. 1 that for same r_s , the distance (x) of the point of intersection of refracted rays will be higher for $2\varphi > 0$ as compared to that for $2\varphi = 0$. Thus the decrease in fringe visibility with the distance from the biprism for a geometrically diverging beam will differ as compared to that for a collimated beam. Also, the line focussing of curved fringes during FBG writing may dilute the fringe visibility, normal to the optical axis. However, the difference in the value of two visibility functions in a fringe plane (x) for a collimated and a diverging beam of small angular envelope ($2\varphi \sim 2^\circ$) is not significant. Typically for $\Delta\phi = 40 \mu\text{rad}$, the Bragg wavelength tunability within the width (Δx) of 7.6 mm in the fringe depth is about 20 nm for $2\varphi = 1^\circ$ and 40 nm for $2\varphi = 2^\circ$. The Bragg wavelength tunability will increase with the decrease in far-field divergence ($\Delta\phi$).

Figure 10 shows the variation of $v(x)$ and $[v(x)L(x)]$ with the increase in distance (x) from biprism for typical inputs $\chi F_0 = 1$, $\Delta\phi = 40 \mu\text{rad}$ and $\beta = 24^\circ$. In this simulation, the variation of fringe visibility transverse to optical axis is ignored. The simulated RI modulation contrast decreased with the increase in distance of FBG writing plane from the biprism. The spectral bandwidth of an inscribed FBG will

decrease with the increase in the distance of the FBG writing plane from the biprism. This is due to the decrease in RI modulation and increase in FBG length with the increase in distance of FBG writing plane from the biprism. Also for a UV beam of large spectral width and non-uniform beam profile, the simulated RI modulation will decrease with the increase in $|z|$ from its value on optical axis ($z = 0$), on account of fringe visibility dilution. Thus reflectivity of a FBG will be comparatively lower for a UV beam of non-uniform profile and of higher spectral width. This dilution of reflectivity may be highest for the FBGs written at the middle of the fringe depth of the biprism where inscribed FBG length is maximum.

3 Experimental method

A silica biprism of refraction angle 24° and 20 mm base width (in xz -plane) was used to study the saturation of RI modulation and reflectivity of FBGs written at different distances from the biprism. The UV beam (repetition rate ~ 5.6 kHz, pulse width ~ 30 ns, spectral band width ~ 12 GHz, average power ~ 300 mW) of diameter of 2.5 mm was generated from β -BBO crystal (Type I, cut angle 50° for $\lambda = 510$ nm)-based second harmonic frequency conversion of copper vapor laser (CVL) ($\lambda = 510$ nm) beam. The beam profile was nearly top hat and far-field average divergence of 10 mm diameter UV beam was about $52 \mu\text{rad}$. The UV beam power stability was of the order of $\pm 3\%$. For FBG writing, the UV beam was expanded to a dimension of 12 mm in the xz -plane by combination of two cylindrical lenses and then directed by a mirror into the biprism. The geometrically diverging envelope (in xz -plane) of the UV beam was changed by changing the distance between the two cylindrical lenses. A cylindrical lens of focal length 75 mm compressed the UV beam to a strip of width about $200 \mu\text{m}$ (in yz -plane) to increase the power density on the fiber. FBGs were inscribed in Ge-B co-doped fiber and hydrogen-loaded SMF-28 single-mode fibers, by placing the fiber parallel to the z -axis. The cylindrical lens position was adjusted so as to keep the spot size nearly same at each writing position. The Bragg wavelength shift ($\Delta\lambda_b$) during fabrication and transmission dip (T_d) was monitored by an optical spectrum analyzer (Agilent 86142B). The length, $L(x)$, of a FBG written at different distances (x) from the biprism is calculated from Eq. (2a). The FBG reflectivity (R) is calculated from the relation, $R = 1 - 10^{-T_d/10}$ where T_d is observed transmission dip. The average RI change ($\langle\Delta n\rangle$) is calculated from the relation, $\langle\Delta n\rangle = n_{\text{eff}} \Delta\lambda_b/\lambda_b$, where n_{eff} is effective refractive index and $\Delta\lambda_b$ is the Bragg wavelength shift during FBG writing. The Bragg wavelength shift ($\Delta\lambda_b$) is calculated from the center wavelength in the FBG traces recorded just after starting

and before stopping of fringe exposure. The RI modulation (Δn_{ac}) is calculated from the relation, $\Delta n_{\text{ac}} = \{\lambda_b/\pi L(x)\} \tanh^{-1}(R^{1/2})$. The RI modulation contrast (ν) is calculated from the ratio of RI modulation to the average effective RI change. The RI modulation and average RI changes are calculated assuming a uniform FBG. The thermal responses of the FBG spectrums were recorded by heating it in in-house built tube ovens. Thermocouple transducer connected to the temperature controller was used to measure the temperature.

The small separation ($\sim 0.53 \mu\text{m}$) of fringes formed in the overlap region of 24° biprism is difficult to resolve by imaging on the CCD due to limitations of resolution optics. As the CCD used was also not UV sensitive, the fundamental CVL beam of diameter 10 mm was used to study the relative trends of variation of fringe visibility and coupling factor in the overlap region of a 2° refraction angle biprism. The use of CVL beam may be reasonable as the spatial coherence characteristics of the second harmonic beam follow those of the fundamental CVL beam [23–25]. The fringes of width $14.6 \mu\text{m}$ formed were magnified by a $100\times$ microscope and imaged by a CCD (Pixelfly qe, PCO AG, pixel size of $6.45 \mu\text{m} \times 6.45 \mu\text{m}$), at different distances from the biprism. The fringe visibility (V) was estimated from the relation, $V = (I_{\text{max}} - I_{\text{min}})/(I_{\text{max}} + I_{\text{min}})$, where I_{max} and I_{min} are intensity at fringe maximum and minimum, respectively.

3.1 Results and discussion

To study the variation of reflectivity, FBGs were written in Ge-B co-doped single-mode fiber (GF1, Nufern: core diameter— $9 \mu\text{m}$, cutoff— 1260 nm, NA-0.13) at different distances from the biprism. At a particular FBG writing fringe plane, the transmission dip of the FBG increased nonlinearly with the increase in accumulated fluence followed by decay after saturation.

Figure 11 shows observed variation of maximum transmission dip and Bragg wavelength shift of FBGs written at different distances from the biprism. The observed maximum reflectivity was 93.6% ($T_d = -12$ dB) for a FBG written at the distance 7 mm. Figure 12 shows the transmission spectrum of this FBG having spectrum bandwidth ~ 0.9 nm, length ~ 3.4 mm and RI modulation $\sim 2.95 \times 10^{-4}$. The observed maximum transmission dip increased as the distance of the FBG writing plane from the biprism increased up to 7 mm. The maximum transmission dip decreased with further increase in the biprism-to-fiber distance beyond 7 mm.

The Bragg wavelength shifts of the FBGs during fabrication at different distances from the biprism were of the order of 0.9 nm, and the writing times were about 250 s (fluence ~ 3 kJ/cm²). The Bragg wavelength increased due

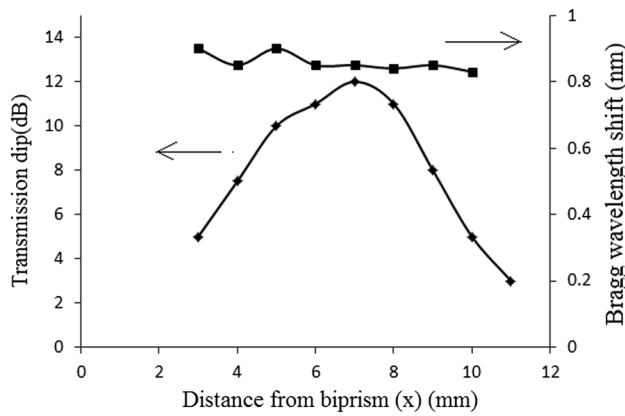


Fig. 11 Variation of transmission dip (T_d) and Bragg wavelength shift ($\Delta\lambda_b$) of FBGs (in GF1 fiber) written at different distances (x) from the biprism

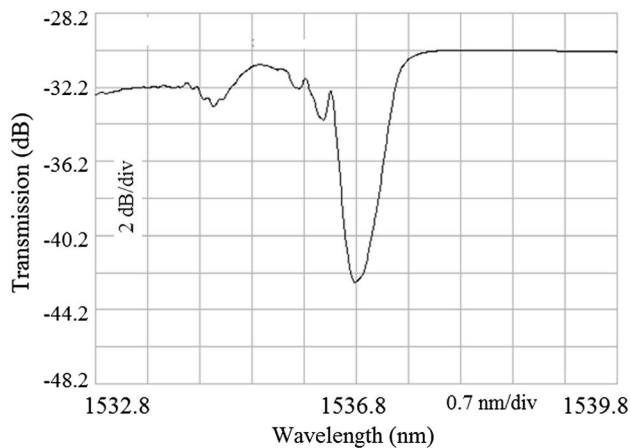


Fig. 12 Transmission spectrum of the FBG (in GF1 fiber) written at a distance of 7 mm from the biprism

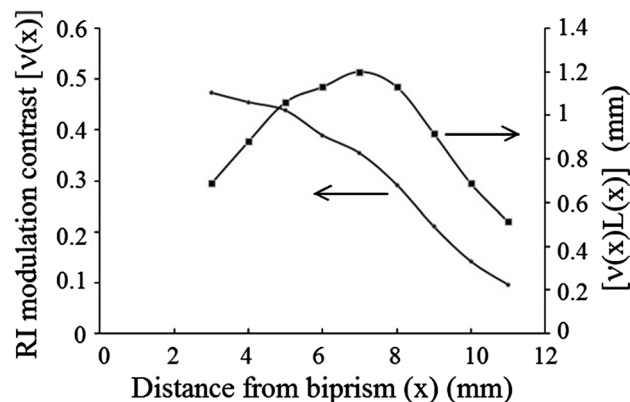


Fig. 13 Variation of $\nu(x)$ and $\nu(x)L(x)$ of FBGs written at different distances (x) from biprism

to increase in average RI index. Figure 13 shows the variation of $[\nu(x)L(x)]$ and RI modulation contrast with the increase x . The error in estimation of $[\nu(x)L(x)]$ is of the order of 5 %. This error is attributed to resolution of OSA and UV power stability. The resolution of OSA in measuring transmission dip is ± 0.01 dB and that in wavelength is ± 10 pm. The UV absorption leads to heating of the fiber. It is observed that the Bragg wavelength of an inscribed FBG increased by about 0.4 nm when illuminated by UV beam of power 300 mW. The power fluctuation of ± 3 % leads to the error of about (\pm) 12 pm in measurement of $\Delta\lambda_b$. The error of about ± 22 pm in observation of $\Delta\lambda_b$ and ± 0.01 dB in T_d leads to error in estimation $\langle \Delta n \rangle$ and Δn_{ac} . Thus the overall error calculated for $\nu(x)$ and $[\nu(x)L(x)]$ is of the order of 5 %. The RI modulation and modulation contrast decreased with the increase in the distance of the FBG writing plane from the biprism. The product of RI modulation contrast and FBG length passed through a maximum.

Figure 14 shows the growth of transmission dip with fluence for FBGs written at distances (x) of 3, 6 and 9 mm from the biprism. The FBG reflectivity is higher for the biprism-to-fiber distance of 6 mm as compared to that for $x = 3$ and 9 mm. The RI modulation estimated from the results decreased with the increase in the distance (x). Typically at a low fluence of 0.5 kJ/cm^2 , the calculated RI modulation values are about 1.8×10^{-4} , 1.4×10^{-4} and 0.78×10^{-4} for FBGs written at 3, 6 and 9 mm, respectively. The UV fringes-induced refractive index modulation decreased with the increase in distance from biprism, in both saturated and unsaturated regime, due to the decrease in fringe visibility. The deviations of experimental and analytical results are attributed to the following reasons. The RI modulation and change in average RI are calculated assuming a uniform FBG. However, the fringe intensity distribution and therefore RI changes also depend on beam profile, beam focussing, interferometer type and the distance of the fringe plane from the beam splitter [26] which has been ignored. The analytical result uses a constant divergence, whereas the divergence of the fundamental CVL and thus the UV beam evolves within the pulse [23–25]. The misalignment of the fiber in the focal plane of the cylindrical lens may lead to tilting of grating planes and consequent loss of coupling coefficient [27].

A 2° biprism employed to study the variation of $\Omega(x)$ experimentally. Figure 15a and b shows the fringe intensity distribution recorded at distance of 20 mm and 120 mm from the apex of the 2° biprism, respectively. The fringe contrast decreased with the increase in the biprism-to-fiber distance. Figure 16 shows the estimated variation of $V(x)$ and $\Omega(x)$ with x . The fringe visibility decreased, whereas coupling factor passed through a maximum with the increase in distance (x) of the fringe plane from the biprism.

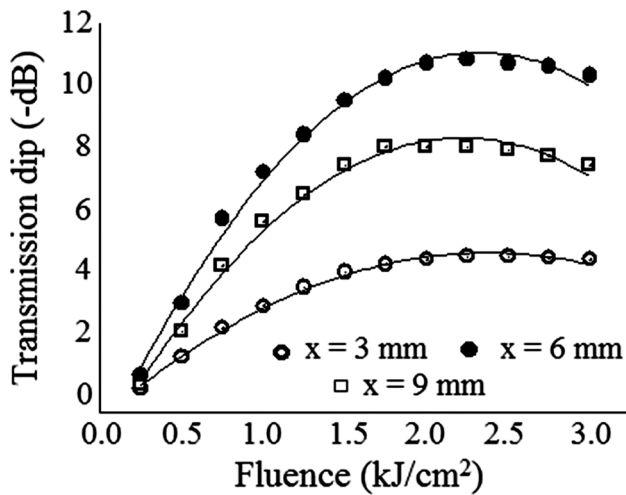


Fig. 14 Growth of transmission dip (T_d) with fluence for FBGs written at 3, 6 and 9 mm from the biprism

The highest value of $\Omega(x)$ is 1.6 mm, observed at about 100 mm from the biprism, whereas the distance (x_0) of center of fringe depth is 142 mm for $\beta = 2^\circ$ and $W = 10$ mm. The experimental trends on $V(x)$ and $\Omega(x)$ agree with analysis. The observed variation of $\nu(x)$ and $[\nu(x)L(x)]$ for FBGs written at different distances from the 24° biprism is similar to the measured trends of $V(x)$ and $\Omega(x)$ for the 2° biprism, but with the reduced distance. An analogy may be established using Eq. (18) for $\beta = 2^\circ$ and 24° for same beam parameters. The reduction in fringe visibility (Eq. 6) along optical axis and the increase in beam overlap length (Eq. 2a) normal to the optical axis with the increase in distance from biprism are higher for $\beta = 24^\circ$ as compared to that for $\beta = 2^\circ$. For same coupling factor, the biprism-to-fringe plane distance for a 24° biprism is approximately 0.063 times (~ 6.25 mm) of that for a 2° biprism. The higher fringe visibility leads to higher value of RI modulation, and the higher value of coupling factor

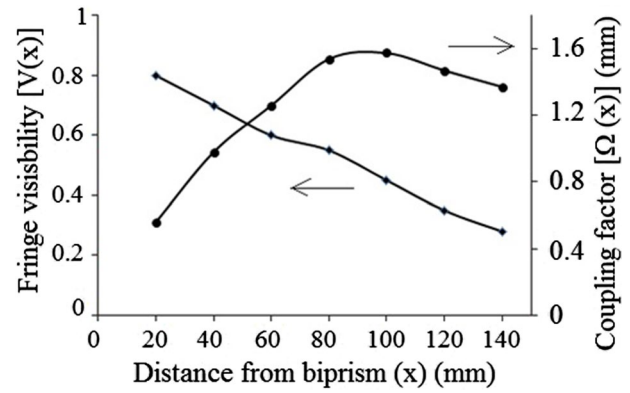


Fig. 16 Variation of $V(x)$ and $\Omega(x)$ with the increase in distance (x) from the 2° biprism

leads to higher value of observed νL . The experimentally observed results qualitatively agree with the analysis based on one-photon absorption presented in Sect. 2.2.

The different reflectivities observed for FBGs in different fibers is attributed to different concentrations of defects and associated structural modification. FBGs were written in hydrogen-loaded SMF-28 fiber. Hydrogen loading enhances the photosensitivity of germanosilicate fibers and yields RI changes (Δn) in excess of 0.011, on exposure to UV radiation [28]. Introduction of interstitial molecular hydrogen to the glass network produces significant quantities of paramagnetic and diamagnetic species upon exposure to intense UV radiation [29]. The hydrogen reacts with Ge ion to form GeH, considerably changing the band structure in the UV region, thus influencing the local refractive index [2]. In the present study, hydrogen loading was carried out at 100 bar pressure at 100°C for 144 h. The hydrogen loading prior to UV irradiation at 255 nm allowed inscription of faster and stronger gratings. Figure 17a, b shows the transmission spectrum of

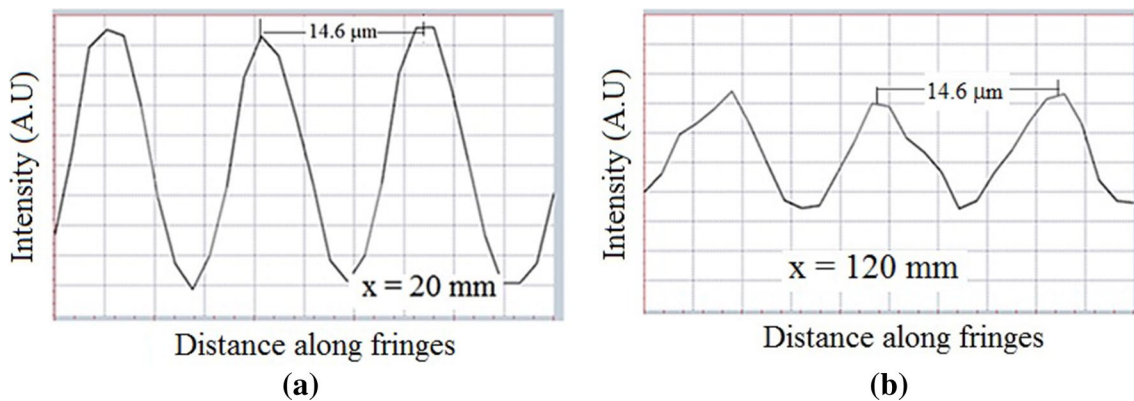


Fig. 15 Fringe intensity distribution at the distance of **a** 20 mm and **b** 125 mm from the 2° biprism

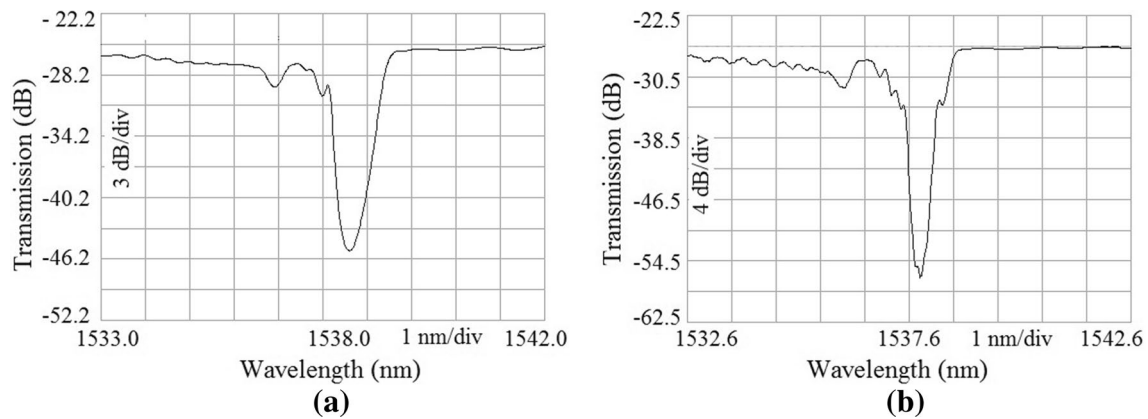


Fig. 17 Transmission spectrum of FBGs in hydrogen-loaded SMF-28 fiber written at distance of **a** 4 mm **b** 7 mm from the biprism

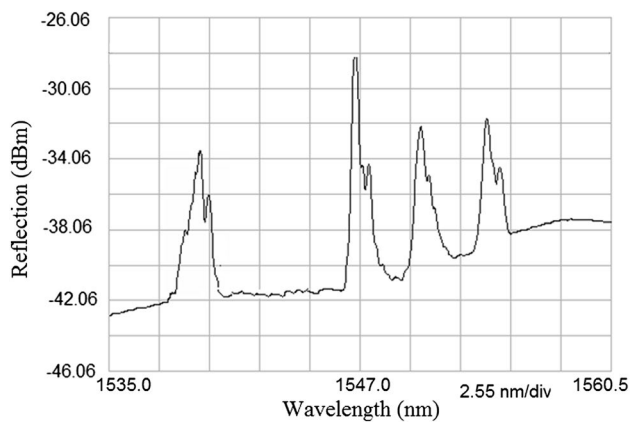


Fig. 18 Reflection spectrum of FBG array (in GF1 fiber) written at different distances from the biprism for a geometrically diverging ($2\varphi \sim 1^\circ$) writing UV beam

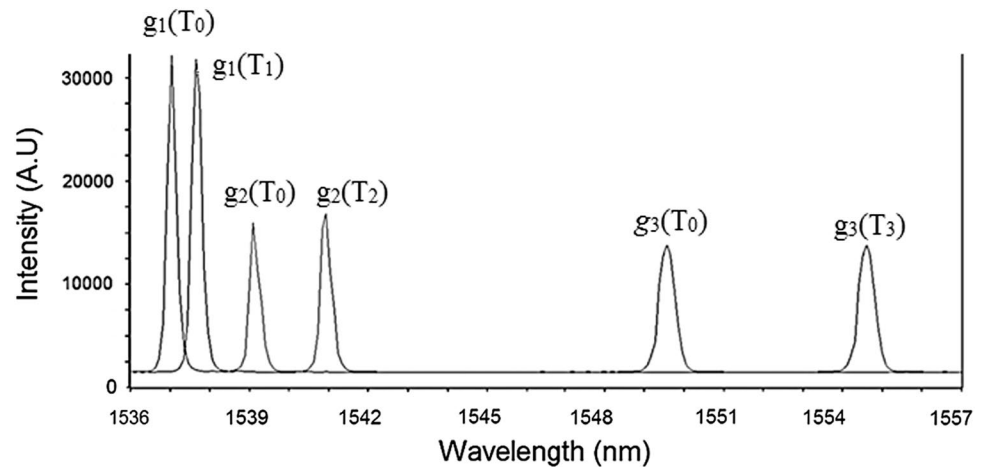
FBGs in hydrogen-loaded SMF-28 fiber written at the distances of 4 mm ($T_d \sim -20$ dB, $R \sim 99\%$, $L \sim 2$ mm, $\Delta n_{ac} \sim 0.76 \times 10^{-3}$) and 7 mm ($T_d \sim -29$ dB, $R \sim 99.8\%$, $\Delta n_{ac} \sim 0.58 \times 10^{-3}$) from the biprism, respectively. The RI modulation decreased with the increase in distance of the FBG writing plane from the biprism. The maximum reflectivity observed was 99.8%, at the fluence of ~ 1.5 kJ/cm².

FBGs of different wavelengths are written in Ge-B co-doped fiber (GF1) by placing the fiber at different distances from the biprism while using geometrically diverging UV beam. Figure 18 shows the typical reflection spectrum of FBGs at different Bragg wavelengths, written by shifting the fiber position, approximately from 4 to 9 mm from the apex of biprism. In this case, the angular envelope (2φ) of the geometrically diverging UV beam was about 1° . With this increase in biprism-to-fiber distance, the Bragg wavelength shifted by about 15 nm. The Bragg resonant

wavelength can also be tuned by changing the geometrical divergence of the incident UV beam. A biprism can be used to write grating arrays used for distributive sensing of different parameters such as strain and temperature. Detailed discussion on distributive sensing is beyond the scope of this paper. However, as a representative for multipoint sensing, Fig. 19 shows the Bragg wavelengths of three FBGs (designated as g_1 , g_2 and g_3) on the same fiber, at reference ($T_0 \sim 25^\circ\text{C}$) and elevated temperatures T_1 (100°C), T_2 (200°C) and T_3 (450°C). The FBG spectrum is recorded by a FBG interrogator (JDSU 8100). The temperature sensitivity is about 10.5 pm/ $^\circ\text{C}$.

The observed higher reflectivity of 93.6% for FBGs in Ge-B co-doped fiber and 99.8% for FBGs in hydrogen-loaded SMF-28 fiber in this study is attributed to the consideration of spatial variation of fringe visibility on the optimization of FBG reflectivity. Maximum reflectivity was observed at the position of maximum coupling factor, not at the fringe plane of maximum FBG length. Experimental results showed that suitably choosing a FBG writing fringe plane in the biprism fringe depth and hydrogen loading can improve fabrication efficiency of FBG writing by a biprism interferometer. Since the biprism is easy to fabricate and cost effective, it can be used to fabricate FBGs for sensing of different parameters as the quantity to be measured is wavelength specific and does not require high reflectivity. The additional advantage is the capability to tune the Bragg wavelength by simply using a geometrically diverging UV beam. The FBG writing by a biprism interferometer has certain disadvantages. It requires UV beams of high temporal and spatial coherence. The FBG writing by this interferometer is alignment sensitive. The misalignment and/or stability of the writing setup may induce Bragg wavelength shift and loss of FBG reflectivity. The diffraction at the sharp edge of the biprism apex may distort the fringe pattern. FBG writing by a geometrically diverging beam of larger envelope will induce chirp

Fig. 19 Bragg wavelength of three FBGs at reference (T_0) and at elevated temperatures



in the FBG. The small length of biprism-written FBG will lead to a broader spectrum. The maximum length of FBGs written by a biprism is half of the UV beam diameter. The FBG length is further reduced by laser beam bandwidth and far-field divergence.

4 Conclusion

The analysis showed that the spatial variation of fringe visibility affects the fabrication efficiency of FBGs written by a biprism interferometer. It is analytically shown that the RI modulation contrast decreases, whereas the reflectivity passes through a maximum with the increase in the distance of FBG writing plane from the biprism. The fringe plane of maximum coupling factor determines the maximum FBG reflectivity. The experimental results confirmed that selection of FBG writing fringe plane in the interference region is crucial to maximize reflectivity in biprism-based FBG writing. The experimental and analytical results agree qualitatively. The observed reflectivity of 93.6 % (12 dB) for FBGs in Ge-B co-doped fiber and 99.8 % (29 dB) for FBGs in hydrogen-loaded SMF-28 fiber are most probably the highest values reported in the field of FBG writing by a biprism interferometer.

References

1. A. Othonos, K. Kalli, *Fiber Bragg Gratings: Fundamentals and Applications in Telecommunications and Sensing* (Artech House, Norwood, 1999)
2. R. Kashyap, *Fiber Bragg Gratings* (Academic, London, 1999)
3. Y. Rao, *Meas. Sci. Technol.* **8**, 355 (1997)
4. G. Meltz, W.W. Morey, W.H. Glenn, *Opt. Lett.* **14**, 823 (1989)
5. T. Erdogan, *J. Light wave Technol.* **15**, 1277 (1997)
6. W. Morey, G.A. Ball, G. Meltz, *Opt. Photonics News* **5**, 8 (1994)
7. K. Hill, B. Malo, F. Bilodeau, D.C. Johnson, *Annu. Rev. Mater. Sci.* **23**, 125 (1993)
8. P. Dyer, R. Farley, R. Gied, *Opt. Commun.* **115**, 327 (1995)
9. C. Li, Y. Lu, S. Wu, Q. Su, C. Huang, *Opt. Laser Technol.* **36**, 459 (2004)
10. W. Wang, J. Grant, A. Sharma, G. Myers, *J. Light Wave Technol.* **19**, 1569 (2001)
11. B. Malo, K. Hill, F. Bilodeau, D. Johnson, J. Albert, *Electron. Lett.* **29**, 1668 (1993)
12. A. Martinez, M. Dubov, I. Khrushchev, I. Bennion, *Electron. Lett.* **40**, 1170 (2004)
13. Q. Zhang, D. Brown, L. Reinhart, T. Morse, *Opt. Lett.* **19**, 2030 (1994)
14. N. Rizvi, M. Gower, *Appl. Phys. Lett.* **67**, 739 (1995)
15. O. Prakash, R. Mahakud, R. Biswal, S. Gurram, H.S. Vora, S.K. Dixit, *Appl. Opt.* **46**, 6210 (2007)
16. W. Xie, M. Douay, P. Bernage, P. Niay, J. Bayon, T. Georges, *Opt. Commun.* **101**, 85 (1993)
17. G. Srikanth, *Appl. Opt.* **47**, 3092 (2008)
18. L. Mandel, E. Wolf, *Rev. Mod. Phys.* **37**, 231 (1965)
19. S. Walborn, C. Monken, S. Pádub, P.S. Ribeiro, *Phys. Rep.* **495**, 87 (2010)
20. E. Wolf, E. Collett, *Opt. Commun.* **25**, 293 (1978)
21. R. Mahakud, O. Prakash, S. Dixit, J. Mittal, *Opt. Commun.* **282**, 2204 (2009)
22. R. Mahakud, O. Prakash, S. Nakhe, S. Dixit, *Appl. Opt.* **51**, 1828 (2012)
23. J.J. Chang, *Appl. Opt.* **33**, 2255 (1994)
24. D.W. Coutts, *IEEE J. Quantum Electron.* **31**, 330 (1995)
25. O. Prakash, S. Dixit, R. Bhatangar, *IEEE J. Quantum Electron.* **38**, 603 (2002)
26. R. Mahakud, J. Kumar, O. Prakash, S.V. Nakhe, S.K. Dixit, *Opt. Commun.* **285**, 5351 (2012)
27. T. Erdogan, J.E. Sipe, *J. Opt. Soc. Am. A* **13**, 296 (1996)
28. R. Atkins, P. Lemaire, T. Erdogan, V. Mizrahi, *Electron. Lett.* **29**, 1234 (1993)
29. K. Awazu, H. Onuki, K. Muta, *J. Non Cryst. Solids* **211**, 158 (1997)